High-pressure luminescence of Cr^{3+}-doped CaO-Ga_2O_3-GeO_2 glasses

M. Grinberg,[1] J. Barzowska,[1] Y. R. Shen,[2] K. L. Bray,[2] B. V. Padlyak,[1,3] and P. P. Buchynskii[4]
[1]*Institute of Experimental Physics, University of Gdańsk, Wita Stwosza Str. 57, 80-952 Gdańsk, Poland*
[2]*Department of Chemistry, Washington State University, Pullman, Washington 99164-4630*
[3]*Department of Physics, Ivan Franko National University of Lviv, Dragomanov Str. 50, 79-005 Lviv, Ukraine*
[4]*Lviv Scientific and Industrial Amalgamation "Karat," Stryjska Str. 202, 79-031 Lviv, Ukraine*
(Received 20 July 2001; published 15 January 2002)

We present ambient-pressure luminescence, luminescence excitation spectra, and luminescence decays and high-pressure luminescence of chromium doped CaO-Ga_2O_3-GeO_2 glass material. The material has been found to be very inhomogeneous with emission of Cr^{3+} ions that are in different coordinated environments. Although the broadband emission dominates the overall emission of Cr^{3+} at ambient pressure, the high-pressure results indicate that the Cr^{3+} luminescence mainly originates from the high-field Cr^{3+} sites and is characteristic of the *R* line emission and the inhomogeneously broadened sideband. The physical quantities of crystal-field strength, Racach parameters, and inhomogeneous crystal-field distribution function have been estimated in the context of a standard configurational coordinate model.

DOI: 10.1103/PhysRevB.65.064203 PACS number(s): 71.70.−d, 78.55.Hx, 62.50.+p

I. INTRODUCTION

Disordered crystal and glass matrices doped with transition-metal and rare-earth ions are still attractive as potential laser media, especially for tunable solid-state lasers[1,2] and optical fibers.[3] Of particular interest is the octahedrally coordinated Cr^{3+} ion. In low-medium strength crystal fields, Cr^{3+} exhibits a broadened luminescence band related to the $^4T_2 \rightarrow {}^4A_2$ spin allowed transition[4–7] or a superposition of the broad $^4T_2 \rightarrow {}^4A_2$ band and the sharper spin forbidden $^2E \rightarrow {}^4A_2$ (*R*-line) transition.[8,9] Structural disorder in glasses results mainly in a broad distribution of the energy of the $^4T_2$ state and inhomogeneous broadening of the $^4T_2 \rightarrow {}^4A_2$ transition. Less significant, but still considerable, inhomogeneous broadening of the $^2E \rightarrow {}^4A_2$ transition is also observed.

In this paper, we present spectroscopic investigations of a member of the CaO-Ga_2O_3-GeO_2 family of glasses. We specifically consider the garnet composition $Ca_3Ga_2Ge_3O_{12}$ ($3CaO$-Ga_2O_3-$3GeO_2$) (CGGG) doped with chromium. The Nd^{3+}-doped crystalline analog, CGGG:Nd^{3+}, is a well-known laser material.[10] The emission spectrum of crystalline CGGG:Cr^{3+} is dominated by the *R* lines of high-field Cr^{3+} sites[11] (commonly referred to as high-field Cr^{3+} sites when the energy of the $^4T_2$ state is higher than that of the ^2E state of Cr^{3+} and as low-field Cr^{3+} sites when the energy of the $^4T_2$ state is lower than that of the ^2E state of Cr^{3+}). In gallogermanate $Ca_3Ga_2Ge_4O_{14}$ ($3CaO$-Ga_2O_3-$4GeO_2$) (CGGO) crystals doped with Cr, Cr^{3+} ions occupy primarily low-field octahedral sites and exhibit primarily broad $^4T_2 \rightarrow {}^4A_2$ emission. Only a small fraction of the Cr^{3+} sites in CGGO are high-field and only weak *R* line emission is observed.[12] Similarly, in the crystalline garnet $Ca_3Sc_2Ge_3O_{12}$ ($3CaO$-Sc_2O_3-$3GeO_2$) (CSGG) doped with chromium, Cr^{3+} ions occupy only low-field octahedral sites.[13]

The effect of inhomogeneous broadening due to structural disorder on the luminescence of Cr^{3+} has been investigated for several gallogermanate crystals,[14–16] aluminosilicate glasses,[6] and congruent $LiTaO_3$.[17] In all of these systems, the disorder is large enough to differentiate the $^4T_2$ state energy by hundreds of wave numbers. Since the energy of the ^2E state is intrinsically much less sensitive to structural variations, its variation over a distribution of structurally inequivalent sites in the presence of structural disorder is much less pronounced. As a result of the disparate effects of disorder on the energies of the ^2E and $^4T_2$ states, it becomes possible for Cr^{3+} to exist as both high field and low field in nominally equivalent crystallographic sites. In such materials, the broadband $^4T_2 \rightarrow {}^4A_2$ emission and the *R*-line emission both contribute to the spectrum, even at very low temperature. Ideally, an analysis of the inhomogeneously broadened spectrum should provide information on the distribution of crystal-field strengths as well as information on low-symmetry distortions from octahedral symmetry induced by structural disorder. In practice, however, the strong homogeneous broadening of the absorption and emission bands between the $^4A_2$ and $^4T_2$ states prevents one from separating the homogeneous and inhomogeneous contributions to the spectrum when low-field Cr^{3+} ions are present. As a result, it is not possible to properly distinguish different sites, to determine the distribution of crystal-field strengths, or to describe low-symmetry distortions.

The ability of high pressure to induce the transitions from low field to high field in Cr^{3+}-doped materials has been previously demonstrated.[18–22] It has been shown that pressure induces an increase in the energy of the $^4T_2$ state of 10–15 cm^{-1}/kbar, whereas the energy of the ^2E state decreases by 1–2 cm^{-1}/kbar. Thus by applying pressure to low-field Cr^{3+} sites, we can induce an electronic crossover of the $^4T_2$-^2E states. As a consequence of the crossover, the broad $^4T_2 \rightarrow {}^4A_2$ emission band disappears and is replaced by the sharp $^2E \rightarrow {}^4A_2$ *R*-line emission. As a result, it becomes possible with pressure to spectrally isolate the *R*-line emission. Since the *R*-line luminescence is weakly broadened, the analysis of its line shape provides information on the number of different sites and the crystal-field strength distribution.[14,17,23] In strongly disordered materials with multiple sites, the broad distribution in the energy of the $^4T_2$ state means that the electronic crossover occurs

over a wide range of pressures. As a result, the broadband and *R*-line emission are simultaneously present over a wide range of pressure. In such systems, an analysis of the pressure dependence of the ratio of the *R*-line intensity to the broadband intensity allows one to determine the distribution function of the $^4T_2$ state energy.

We have previously reported the emission, luminescence excitation, and high-pressure luminescence spectra of Cr^{3+}-doped CaO-Ga_2O_3-GeO_2 glass.[24] The luminescence consisted of the *R*-line emission at about 690 nm and a much stronger $^4T_2 \rightarrow {}^4A_2$ emission band with a peak at about 800 nm. To resolve the *R*-line and $^4T_2 \rightarrow {}^4A_2$ emission bands, we measured the luminescence of the material under high hydrostatic pressure. We found that the energy of the *R*-line emission decreased with pressure by 1.73 cm^{-1}/kbar, whereas the $^4T_2 \rightarrow {}^4A_2$ emission band was unexpectedly almost independent of pressure.[24] In this paper we present a more complete spectroscopic investigation of luminescence decays, luminescence excitation, and high-pressure luminescence spectroscopy of the Cr^{3+}-doped CaO-Ga_2O_3-GeO_2 glass. Specifically, we have analyzed the broadband emission and its dependence on pressure at variable temperature over a broader spectral range.

II. PREPARATION OF GLASS SAMPLES

Cr-doped glasses of the CaO-Ga_2O_3-GeO_2 system with high chemical purity and optical quality and different stoichiometric compositions were obtained in corundum crucibles by standard high-temperature synthesis methods.[25] The Cr^{3+} was added to the glass composition in the form of $CrCl_3$ liquid solution in amount ranging from 0.01–0.2 wt %. The CaO-Ga_2O_3-GeO_2 system has three stable crystalline forms: $Ca_3Ga_2Ge_3O_{12}$ (ordered garnet structure, space group $Ia3d$), $Ca_3Ga_2Ge_3O_{14}$ (substitutionally disordered Ca-gallogermanate structure, space group $P321$), $Ca_2Ga_2GeO_7$ (gelenite structure, space group $P\bar{4}2_1m$), and respective vitreous forms with compositions similar to these crystalline forms.[25] The chemical composition of the glasses was determined by x-ray microanalysis using a ''Camebax'' apparatus. Glasses with stoichiometric compositions similar to that of calcium-gallium-germanium garnet ($Ca_3Ga_2Ge_3O_{12}$) were selected for spectroscopic investigations and analysis. X-ray diffraction showed that the product obtained in the synthesis was heterogeneous and consisted primarily of a glassy phase with small amount of crystalline precipitates.[26]

III. AMBIENT PRESSURE LUMINESCENCE OF BULK SAMPLES

Argon and He-Ne laser excitation were used in the luminescence and the resulting spectra were corrected for instrumental response. Throughout this paper, the reported emission spectra were obtained by dividing the corrected emission intensity by the third power of photon energy. By normalizing the spectra in this way, the energy of the maximum of the spectrum is equal to the energy of the Frank-Condon transition.

The ambient pressure emission in the bulk sample was found to depend on excitation energy as well as temperature. Luminescence spectra obtained under various conditions are presented in Figs. 1(a) and 1(b). At room temperature [Fig. 1(a)], the luminescence spectra consisted of a broadband peaking at 12 000–13 000 cm^{-1} and a weaker sharp line peaking at 14 480 cm^{-1}. We observed that the relative intensity of the sharp line to the broadband depends weakly on the excitation wavelength. The sharp line is strongest upon 457.9-nm excitation and weakest upon 488-nm excitation. Qualitatively different emission spectra were obtained when the temperature was decreased to 20 K. The sharp line and broadband emission features are still observed at 20 K, but the line shapes and peak energies changed significantly. The maximum of the broadband shifted to $\sim$10 300 cm^{-1} [Fig. 1(b)]. The sharp line broadened and shifted to $\sim$14 230 cm^{-1} [Fig. 1(b)]. An excitation wavelength dependence of the spectrum was also observed at 20 K. Under 514.5-nm excitation (and to some extent, under 488-nm excitation as well), it appeared that the spectral structure observed at room temperature (the line at 14 480 cm^{-1} and the broadband 12 000–13 000 cm^{-1}) still contributed to the 20-K spectrum. By contrast, the room-temperature spectrum obtained under 632.8-nm excitation appeared to include a low-

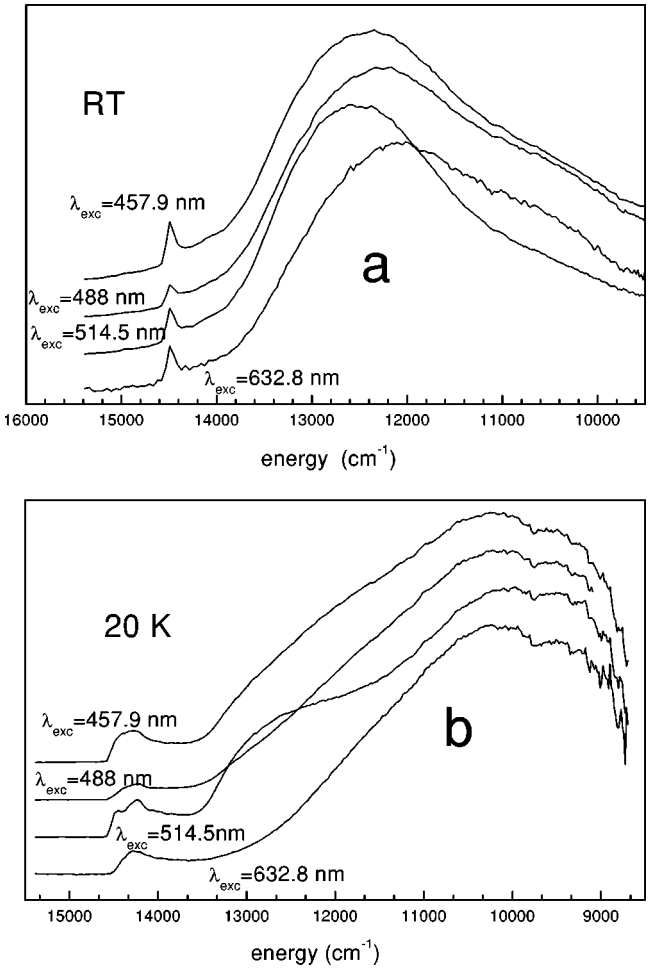

FIG. 1. Ambient pressure luminescence spectra of a bulk sample of CGGG:Cr^{3+} glass obtained at different excitation wavelengths: (a) room temperature and (b) 20 K.

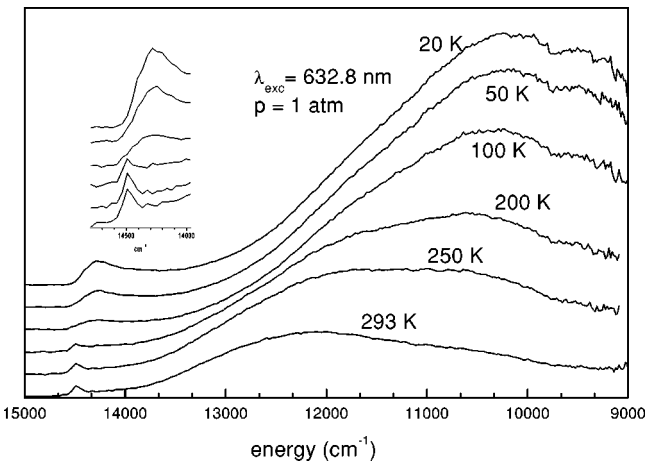

FIG. 2. Ambient pressure luminescence spectra of a bulk sample of CGGG:Cr^{3+} glass obtained at different temperatures upon 632.8-nm excitation. The *R*-line luminescence is presented in the inset.

energy (10 000–11 000 cm^{-1}) contribution from the 20-K broadband feature.

It is interesting to compare the spectra obtained under 632.8-nm excitation at different temperatures (see Fig. 2). At lower temperatures (20, 50, and 100 K), one can see emission features characteristic of the low-temperature spectra at all excitation wavelengths: the broadband peaking at 10 300 cm^{-1} and the sharper line at 14 230 cm^{-1}. Both of these features disappeared with increasing temperature (the sharper band disappeared before the broadband). For temperatures above 200 K, the sharper band at 14 230 cm^{-1} was completely replaced by a band at 14 480 cm^{-1} whose intensity increased with increasing temperature. In the lower energy region, the band at 10 300 cm^{-1} was gradually replaced by the band at 12 000 cm^{-1}. Both broadband features, however, contributed to the spectrum over the entire temperature range of the study. Both broadbands exhibited strong blue shifts with increasing temperature.

The results indicate that the emission is dominated by different Cr^{3+} centers. The ambient pressure emission spectra obtained at room temperature presented in Fig. 1(a) can be interpreted as follows. The sharp line is due to *R*-line emission ($^2E \rightarrow {}^4A_2$) from high-field octahedrally coordinated Cr^{3+} sites. The relatively large linewidth of the *R* line as well as its slightly asymmetric line shape are attributed to inhomogeneous broadening of the transition due to disorder of the host. As far as the broadband is concerned, its energy and line shape are consistent with an assignment to the $^4T_2 \rightarrow {}^4A_2$ transition of low-field octahedrally coordinated Cr^{3+} sites.

At 20 K [Fig. 1(b)], the *R* line at 14 480 cm^{-1} at room temperature was replaced by a broader band peaking at 14 230 cm^{-1}. We attribute the feature at 14 230 cm^{-1} to $^2E \rightarrow {}^4A_2$ emission of Cr^{3+} sites in a glassy environment. The larger linewidth is a consequence of the much more significant inhomogeneous broadening in a glassy phase relative to a disordered crystalline phase.[27] The qualitative and quantitative spectral changes observed with temperature (Fig. 2) are due to energy transfer between the different Cr^{3+} centers and nonradiative processes in the glassy phase.

IV. PRESSURE CALIBRATION

For high-pressure spectroscopy measurements, the sample was powdered and individual pieces were placed in the gasket hole of a diamond-anvil cell. Samples with dimensions of 75–100 μm were selected for the high-pressure studies. We noticed that different glass samples selected for high-pressure experiments had already at ambient pressure different luminescence characteristics. We have distinguished brighter samples with luminescence features similar to those observed in the bulk sample at high temperature (*R* line at 14 480 cm^{-1} and broadband peaking at 12 700 cm^{-1}) and weakly emitting pieces whose emission consisted mainly of the lower energy (10 000–11 000 cm^{-1}) broadband emission.

Experiments have been performed using two sets of experimental systems. For pressure calibration, the CaO-Ga_2O_3-GeO_2 glass sample and ruby crystal were placed in a diamond-anvil cell ''Diacold04'' (modified Merrill-Basset design) made by Diacell Products. Emission light was dispersed by a 2-m monochromator (adapted from a spectrograph, PGS2, Carl Zeiss Jena), equipped with a 651 grooves/mm grating, and detected by a photon counting technique using a Hamamatsu R943-02 photomultiplier tube (PMT). For detailed investigations of the broadband emission, another detection system was used. The emission was dispersed by a 1-m spectrometer (SPEX 1704) and detected with Hamamatsu R2228 PMT. This system had less dispersion, but was sensitive up to 1200 nm. A 4:1 methanol:ethanol mixture or a spectroscopic oil (poly-dimethylsiloxane) was used as the pressure transmitting medium. In the present high-pressure luminescence experiments, the well-known *R*-doublet lines and the symmetric line shapes of ruby indicated a quasihydrostatic pressure distribution was maintained up to 150 kbar.

Using the former experimental system, we were able to measure the ruby R_1 and R_2 lines and the *R* line emission from glass samples with much better than single wavenumber resolution. Since the ruby R_1 and R_2 emission strongly overlap with the *R* lines of the glass we focused the excitation light separately on the ruby and the sample to minimize interference of the luminescence signals. Given the much stronger luminescence intensity of ruby, its emission was still excited by scattered light when we focused on the sample. Consequently, at a given pressure we could observe the ruby luminescence only or luminescence that was a superposition of the ruby and sample luminescence [Figs. 3(a) and 3(b)]. We were able to subtract the ruby emission from the spectrum to obtain the spectrum presented in Fig. 3(c). We found that the energy of the *R*-line luminescence of the CGGG:Cr^{3+} glass sample depends linearly on pressure. The observed pressure shift was found to be equal to -1.73 cm^{-1}/kbar. The data are summarized in Fig. 4. By correlating the *R*-line energy of the CGGG:Cr^{3+} glass sample with the ruby *R* lines, we can use the glass as a secondary pressure calibration standard.

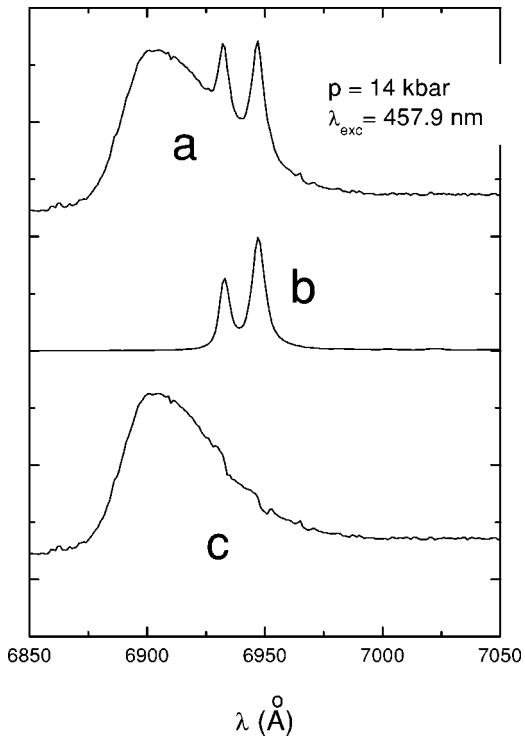

FIG. 3. *R*-line luminescence of a CGGG: Cr^{3+} glass sample and ruby in a diamond-anvil cell. (a) spectrum obtained when the excitation beam was focused on the CGGG:Cr^{3+} sample; (b) spectrum obtained when the excitation beam was focused on ruby; and (c) the resulting CGGG:Cr^{3+} *R*-line luminescence obtained by subtracting out the ruby *R*-line emission features.

For the brighter type of CGGG:Cr^{3+} glass samples, we measured high-pressure luminescence spectra without using ruby and used the pressure shift of the *R*-line emission of the glass sample for pressure determination. When we investigated the weaker emitting samples that exhibited only the broadband emission near 10 000–11 000 cm^{-1} (see above), we used ruby as the pressure indicator.

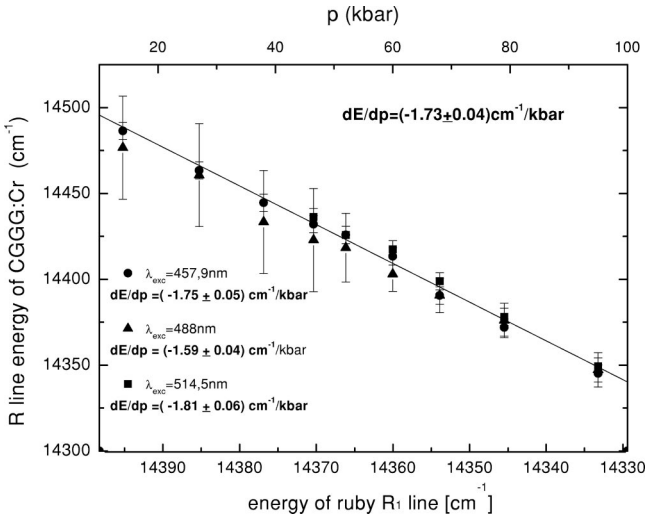

FIG. 4. Variation of the energy of the *R* line of CGGG:Cr^{3+} and the R_1 line of ruby with pressure at room temperature.

V. HIGH-PRESSURE LUMINESCENCE

Figure 5 shows the luminescence spectra of the bright sample obtained for several pressures at room temperature [Figs. 5(a)–5(c)] and at 20 K [Figs. 5(d)–5(f)]. At room temperature, the emission spectrum retains its ambient pressure appearance upon increasing pressure. As discussed above, the *R* lines exhibit a redshift. The pressure shift of the broad emission band is more difficult to determine because of uncertainty in determining the peak maximum. The variation of the estimated broadband peak maximum with pressure is shown in Fig. 6. Although there is some variability, the data indicate a weak redshift of the peak maximum with pressure. From the data, we estimate a redshift of approximately 2 cm^{-1}/kbar. The magnitude of the broadband redshift is similar to that observed for the *R* lines and is much different than the $\sim$10-cm^{-1}/kbar blueshift typically observed for the $^4T_2 \rightarrow {}^4A_2$ emission of Cr^{3+} in crystalline oxides. The shift behavior of the broadband emission of CGGG:Cr^{3+} glass suggests that the emission is not due to the $^4T_2 \rightarrow {}^4A_2$ transition of low-field Cr^{3+} sites.

The low-temperature luminescence decay curves at ambient pressure and room temperature are shown in Fig. 7. Decay curves upon excitation at 532 nm with double frequenced YAG:Nd laser and monitored at several wavelengths are shown. The monitored wavelengths were selected within both the *R*-line and broadband portions of the spectrum. The decay curves at all monitored wavelengths are similar and are well represented by a double exponential function with a long component of $\sim$2.5 ms and a short component of ~ 1 μs. The similar decay behavior of the *R*-line and broadband emission is a further indication that the broadband emission is not due to the $^4T_2 \rightarrow {}^4A_2$ transition of low-field Cr^{3+} sites. The latter transition has a typical lifetime of $\sim$10–$\sim$100 μs in crystalline oxides.

Figure 8 depicts the pressure variation of the ratio of the integrated *R*-line intensity to the combined integrated intensity of the *R*-line and broadband emission. The data indicate a weak variation of the intensity ratio with pressure at room temperature and 20 K for several excitation wavelengths. Small increases in the intensity ratio at 20 K and room temperature upon 488 and 514.5 nm excitation were observed and a small decrease in the intensity ratio was observed at 20 K upon 457.9-nm excitation. The weak variation in intensity ratio observed in CGGG:Cr^{3+} glass is in contrast to the large increase in intensity ratio observed in $LiTaO_3:Cr^{3+}$.[17] This large increasing of the *R*-line intensity in $LiTaO_3:Cr^{3+}$ was attributed to a pressure-induced $^4T_2$-^2E excited-state electronic crossover. Due to disorder in the crystal, the crossover occurred over a wide range of pressure. The intensity ratio in $LiTaO_3:Cr^{3+}$ also showed a strong temperature dependence due to a thermal population of higher vibrational $^4T_2$ states. The absence of a strong intensity ratio variation in CGGG:Cr^{3+} glass with pressure or temperature is a further indication that the broadband emission observed in CGGG:Cr^{3+} is not due to the $^4T_2 \rightarrow {}^4A_2$ transition of low-field sites.

Figure 9 shows the pressure dependence of the emission spectrum of a sample selected from the weakly emitting portion of the heterogeneous bulk sample. The sample retains its

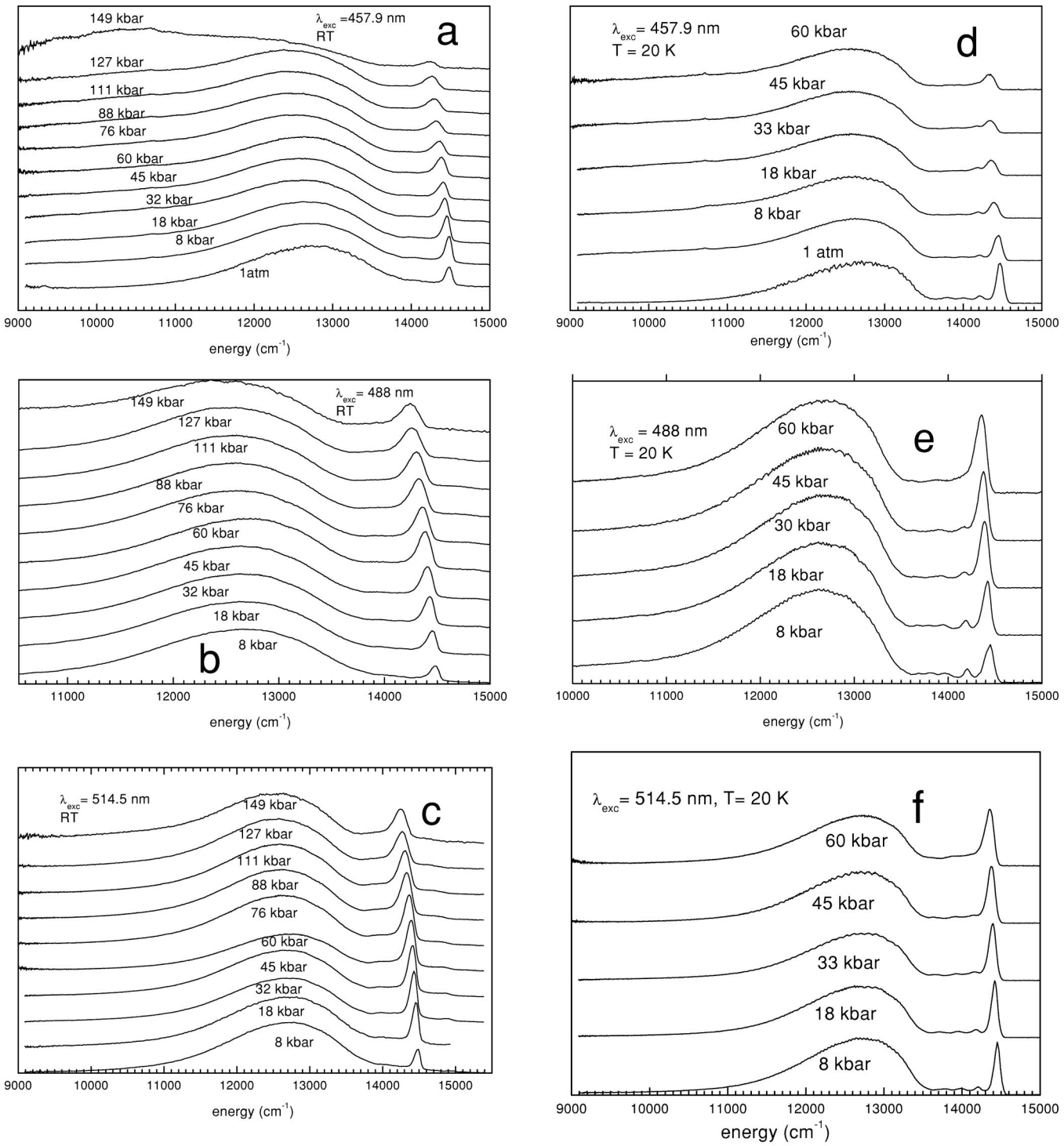

FIG. 5. High-pressure luminescence spectra of CGGG:Cr^{3+} glass at several excitation wavelengths. The sample used in the experiment was selected from a bright portion of the heterogeneous bulk sample: (a) $\lambda_{exc}=457.9$ nm, RT; (b) $\lambda_{exc}=488$ nm, RT; (c) $\lambda_{exc}=514.5$ nm, RT; (d) $\lambda_{exc}=457.9$ nm, 20 K; (e) $\lambda_{exc}=488$ nm, 20 K; (f) $\lambda_{exc}=514.5$ nm, 20 K. RT=room temperature.

broadband appearance and exhibits a redshift with increasing pressure.

VI. BULK SAMPLE EXCITATION SPECTRA

In order to obtain information about the higher excited states of CGGG:Cr^{3+} glass, we completed luminescence excitation measurements on the bulk heterogeneous sample at ambient pressure. The excitation spectra obtained at room temperature and 85 K upon monitoring emission at 14 480 cm^{-1} (*R* line) and 12 700 cm^{-1} (broadband) are shown in Fig. 10. The excitation spectrum at 85 K obtained upon monitoring the emission at 14 480 cm^{-1} consisted of two broad Gaussian shaped bands. An analysis of the spec-

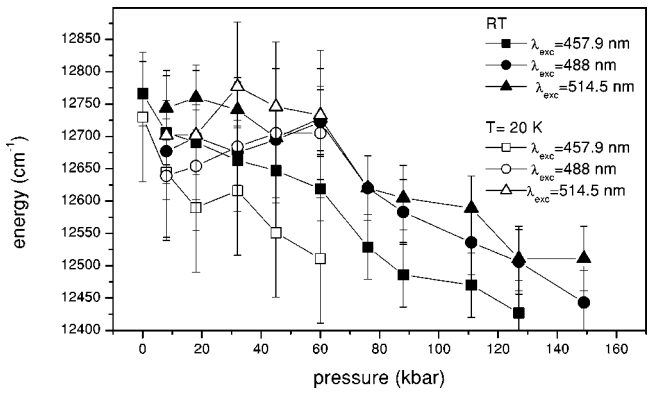

FIG. 6. Pressure variation of the estimated peak maximum of the broadband portion of the spectra shown in Fig. 5.

trum indicates that it contains a band at 17 450 cm^{-1} with a standard dispersion $\sigma = 1090$ cm^{-1} and bandwidth of 2567 cm^{-1} and a band at 23 720 cm^{-1} with a standard dispersion $\sigma = 1150$ cm^{-1} and bandwidth of 2708 cm^{-1}. Both bands exhibited a temperature shift of about -1.5 cm^{-1}/K between 85 K and room temperature. These spectra are consistent with the existence of the high-field Cr^{3+} ions in octahedral coordination. The low- and high-energy excitation bands can be attributed to the $^4A_2 \rightarrow {}^4T_2$ and $^4A_2 \rightarrow {}^4T_1$ transitions, respectively, of high-field Cr^{3+} sites in CGGG:Cr^{3+} glass. From the positions of the excitation bands and the energy of the *R* lines, we can calculate the crystal-field parameters. From the data, we obtain $10Dq = 17\,450$ cm^{-1}, $B = 627$ cm^{-1}, and $C = 3253$ cm^{-1} for the high-field sites.

The excitation spectra of the broadband emission (12 700 cm^{-1}) are similar to those of the *R*-lines (Fig. 10). The lower energy band has a maximum at 17 450 cm^{-1} at 85 K. The energy and bandwidth of the band were nearly temperature independent. The high-energy excitation band observed upon monitoring the broadband emission is more intense and broader than the corresponding band obtained upon monitoring the *R*-line emission. The broadening is a consequence of a readily noticeable shoulder in the excitation band. Instead of a single Gaussian, the high-energy excitation band observed upon monitoring the broadband emission can be resolved into two Gaussian components: one component with a peak at 22 270 cm^{-1} and a standard dispersion $\sigma = 1015$ cm^{-1} and a second component with a peak at 24 000 cm^{-1} and a standard dispersion $\sigma = 1700$ cm^{-1}. The lower energy band at 17 450 cm^{-1} and Gaussian component at 24 000 cm^{-1} observed upon monitoring the broadband emission are similar to features observed upon monitoring *R*-line emission and are attributed to $^4A_2 \rightarrow {}^4T_2$ and $^4A_2 \rightarrow {}^4T_1$ transitions of Cr^{3+}, respectively. The Gaussian component at 22 270 cm^{-1} is likely not related to Cr^{3+}.

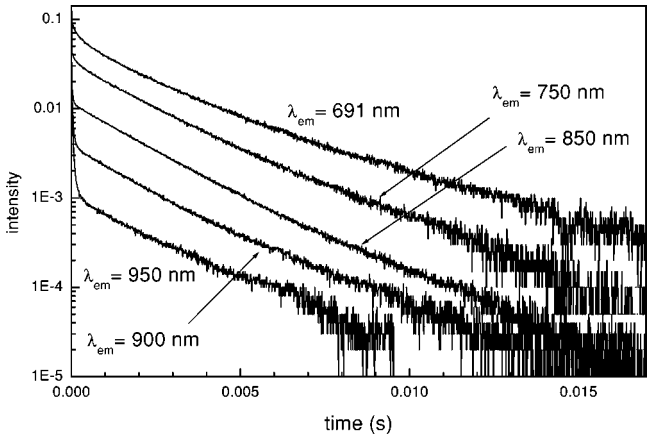

FIG. 7. Luminescence decay curves of a sample of CGGG:Cr^{3+} selected from a bright portion of the heterogeneous bulk sample. The decay curves were obtained at 20 K and ambient pressure upon excitation at 532 nm.

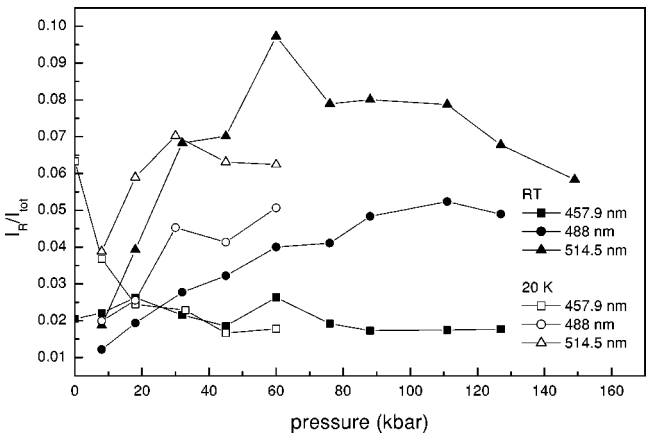

FIG. 8. Ratio of the integrated *R*-line intensity to the total integrated intensity of Cr^{3+} in CGGG glass at room temperature and 20 K as a function of pressure for different excitation wavelengths.

VII. CONFIGURATIONAL COORDINATE DIAGRAM OF HIGH-FIELD OCTAHEDRALLY COORDINATED CHROMIUM CENTER

The crystal-field parameters $10Dq$, *B*, and *C* calculated from the excitation spectrum of the *R*-line emission do not

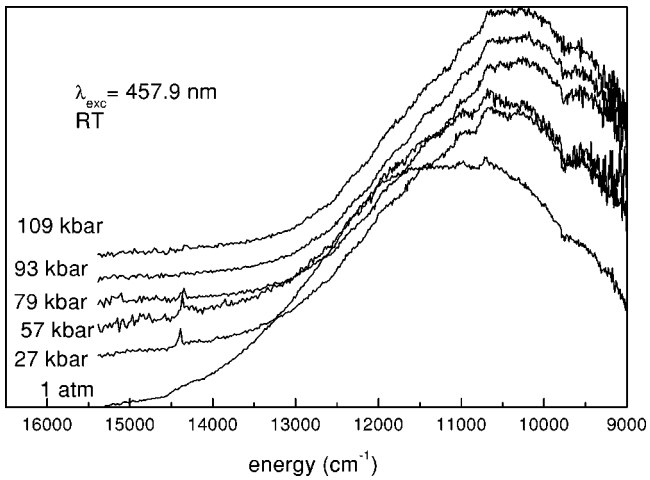

FIG. 9. High-pressure luminescence spectra of CGGG:Cr^{3+} glass at $\lambda_{exc} = 457.9$ nm. The sample used in the experiment was selected from a weakly emitting portion of the heterogeneous bulk sample.

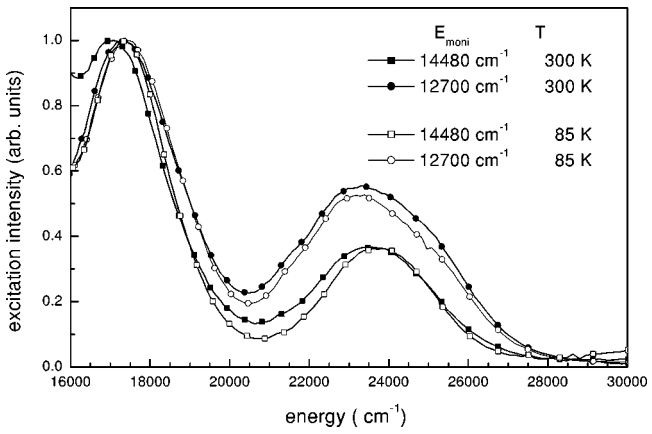

FIG. 10. Ambient pressure luminescence excitation spectra of a bulk heterogeneous sample of CGGG:Cr^{3+} glass at 85 K and room temperature. The spectra were obtained by monitoring *R*-line (14 480 cm^{-1}) and broadband emission (12 700 cm^{-1}).

account for electron-lattice coupling. Since the ground $^4A_2$ state and the excited $^4T_2$ state belong to different electronic configurations (t^3 and t^2e), respectively, the excited-state system relaxes due to lattice rearrangement. Thus the relaxed excited $^4T_2$ state responsible for the $^4T_2 \rightarrow {}^4A_2$ emission has an energy much lower than $10Dq$. This effect is most readily visualized in a configurational coordinate diagram [Fig. 11(a)]. In a one-dimensional approximation, the lattice relaxation is described by a single parameter $S\hbar\omega$ where S is the Huang-Rhys factor that quantifies the electron-phonon coupling strength and $\hbar\omega$ is the energy of the effective local phonon mode.[28] We do not have direct information on the energy minimum of the $^4T_2$ states since the broad emission band observed at $\sim$12 700 cm^{-1} does not correspond to $^4T_2 \rightarrow {}^4A_2$ emission. If the broadband emission did correspond to $^4T_2 \rightarrow {}^4A_2$ emission, we could estimate the position of the zero phonon energy of the $^4T_2$ state as the average of the broadband emission maximum ($\sim$12 700 cm^{-1}) and the $^4A_2 \rightarrow {}^4T_2$ maximum (17 450 cm^{-1}) observed in the excitation spectrum. We could also estimate the electron-lattice coupling energy $S\hbar\omega$ to be half of the difference between the two maxima. If we were to proceed according to the assumption that the broadband emission did correspond to $^4T_2 \rightarrow {}^4A_2$ emission from the Cr^{3+} sites, we would find that the $^4T_2$ zero phonon energy equaled $\sim$15 075 cm^{-1} and that $S\hbar\omega = \sim$2375 cm^{-1}. The resulting hypothetical $^4T_2$ minimum in the configuration coordinate diagram would be about $\sim$600 cm^{-1} higher in energy than the ^2E minimum. Under this scenario therefore the sites would emit primarily through the $^2E \rightarrow {}^4A_2$ transition and any $^4T_2 \rightarrow {}^4A_2$ emission would occur through thermal population of the $^4T_2$ state. Since thermal population of the $^4T_2$ state would require overcoming a 600-cm^{-1} activation barrier, we would expect the $^4T_2$ emission to be strongly temperature dependent under this scenario. The experimental data, however, indicate that the broadband emission intensity does not vary appreciably with temperature relative to the *R*-line emission intensity. We therefore further conclude that the broadband emission at 12 700 cm^{-1} is not due to the $^4T_2 \rightarrow {}^4A_2$ transition in the high-field sites.

We can estimate the energy of the electron-lattice coupling $S\hbar\omega$ of the high-field system in the $^4T_2$ excited state by considering the standard dispersion σ of the homogeneously broadened excitation band (17 450 cm^{-1}) due to the $^4A_2 \rightarrow {}^4T_2$ transition obtained upon monitoring the *R*-line emission at 14 480 cm^{-1} (Fig. 10). Using standard configuration coordinate model analysis,[28] we know the temperature dependence of the homogeneous broadening σ_{hom} as follows:

$$S\hbar\omega = \frac{\sigma_{\mathrm{hom}}^2(T)}{\hbar\omega}\tanh\left(\frac{\hbar\omega}{2kT}\right). \tag{1}$$

When analyzing the CGGG:Cr^{3+} glass, we need to consider the inhomogeneous broadening as well as the homogeneous broadening of the excitation spectrum. If we assume that both the distribution of crystal-field strengths and the homogeneous broadening of the spectrum are given by Gaussian functions, we can relate the standard dispersion σ of the experimental excitation spectrum to the homogeneous and inhomogeneous contributions through

$$\sigma = \sqrt{\sigma_{\mathrm{hom}}^2 + \sigma_{10\mathrm{Dq}}^2}, \tag{2}$$

where $\sigma_{10\mathrm{Dq}}$ is the standard dispersion of the inhomogeneous crystal-field strength distribution for high-field Cr^{3+} sites in

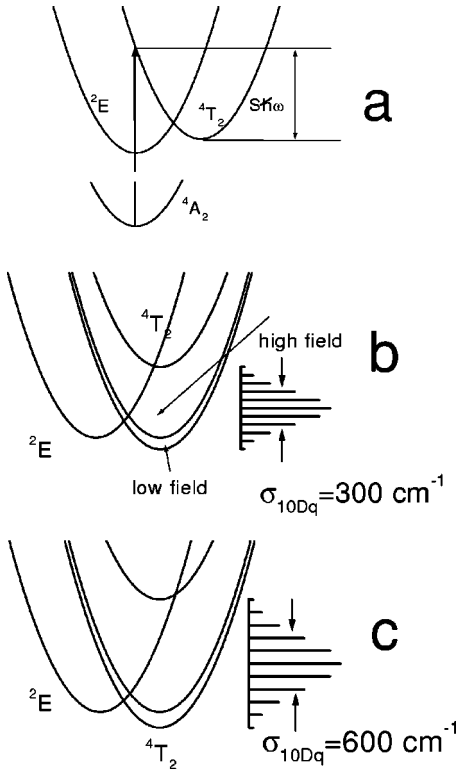

FIG. 11. Configurational coordinate diagrams of Cr^{3+}: (a) system without inhomogeneous broadening of the $^4T_2$ energy; (b) and (c) system with inhomogeneous broadening characterized by standard dispersions $\sigma_{10\mathrm{Dq}} = 300$ cm^{-1} and $\sigma_{10\mathrm{Dq}} = 600$ cm^{-1}, respectively, of the $^4T_2$ energy. Histograms represent the $^4T_2$ state energy distribution functions.

TABLE I. Electron-lattice coupling energy $S\hbar\omega$ obtained for various values of the standard dispersion σ_{10Dq} of the inhomogeneous crystal-field strength distribution for high-field Cr^{3+} sites in CGGG:Cr^{3+} glass. σ_{hom}, the standard dispersion of the homogeneous contribution to the $^4A_2 \rightarrow {}^4T_2$ excitation bandwidth, was calculated for each value of σ_{10Dq} using Eq. (2) and the standard dispersion $\sigma = 1090\ cm^{-1}$ of the experimental $^4A_2 \rightarrow {}^4T_2$ excitation band (room temperature) of the high-field Cr^{3+} sites in CGGG:Cr^{3+} glass. $S\hbar\omega$ was calculated using σ_{hom} and Eq. (1) using $\hbar\omega = 300\ cm^{-1}$.

σ_{10Dq} (cm^{-1})	0	200	300	400	500	600
σ_{hom} (cm^{-1})	1090	1071	1048	1014	969	910
$S\hbar\omega$(cm^{-1})	2403	2320	2222	2080	1900	1675

CGGG:Cr^{3+} glass. Table I summarizes the calculated values of $S\hbar\omega$ for several representative values of σ_{10Dq}. σ_{hom} was calculated from Eq. (2) and the standard dispersion $\sigma = 1090\ cm^{-1}$ obtained from a Gaussian fit of the experimental $^4A_2 \rightarrow {}^4T_2$ excitation band (room temperature) for high-field Cr^{3+} sites (Fig. 10). $S\hbar\omega$ was further calculated from Eq. (1) using $\hbar\omega = 300\ cm^{-1}$. The resulting configuration coordinate diagram for $\sigma_{10Dq} = 300\ cm^{-1}$ and $\sigma_{10Dq} = 600\ cm^{-1}$ are depicted in Figs. 11(b) and 11(c), respectively. The histograms represent the $^4T_2$ state energy distribution functions. Thus single configuration coordinate curves for the ^2E state and the $^4T_2$ state show the existence also of the low-field Cr^{3+} site. The two curves correspond to the upper and lower bounds of the distribution of $^4T_2$ energies resulting from the stated values of σ_{10Dq}. From the diagrams, we see that only a small fraction of high-field Cr^{3+} sites has a minimum $^4T_2$ energy below the ^2E state.

In order to estimate the actual value of the standard dispersion of inhomogeneous broadening of the $^4T_2$ energy in the present CGGG:Cr^{3+} system, we must consider the temperature dependence of the bandwidth of excitation spectrum. From the spectra presented in Fig. 10, we see that the bandwidth (standard dispersion) of the $^4A_2 \rightarrow {}^4T_2$ transition depends weakly on temperature. Only a 15% increase in bandwidth was observed between 85 K and room temperature. Since the homogeneous contribution to the bandwidth is temperature dependent, while the inhomogeneous contribution is not, the weak temperature dependence of the linewidth indicates that inhomogeneous broadening is significant. Using Eqs. (1) and (2) with $\hbar\omega = 300\ cm^{-1}$ and the experimental bandwidths at 85 and 293 K, we estimate $\sigma_{10Dq} = 600\ cm^{-1}$. This broad predicted distribution of the energy of the $^4T_2$ state due to the inhomogeneous crystal-field strength distribution is supported by the significant broadening observed for the $^2E \rightarrow {}^4A_2$ transition in CGGG:Cr^{3+} glass relative to other systems.

We have previously shown in the disordered $LiTaO_3$:Cr^{3+} crystal that an inverse correlation of the $^4T_2$ and ^2E energies exists for crystallographically equivalent sites. This correlation was described by the formula[17]

$$E_{^2E} - E^0_{^2E} = -K(E_{^4T_2} - E_{^4T_2}). \quad (3)$$

Equation (3) relates the distribution function of the $^4T_2$ energy to the distribution of the ^2E energy, or equivalently the R_1 linewidth. For $LiTaO_3$:Cr^{3+}, the coefficient K was found to be of the order of 0.1 for each of the two groups of inequivalent of sites. If we use a similar value of K for CGGG:Cr^{3+} and the experimental dispersion $\sigma_{R_1} = 38\ cm^{-1}$ for the R_1 line, Eq. (3) would predict a standard dispersion $\sigma_{10Dq} = 380\ cm^{-1}$ for the $^4T_2$ energy. This value is smaller than that obtained from the temperature analysis of the excitation band. The difference is not unexpected, however, since the excitation spectrum provides the information about all sites, while the luminescence spectrum provides information only on those sites that were effectively excited by monochromatic light. Our main conclusion at this time is that the approximate values of σ_{10Dq} obtained in this work indicates that $^4T_2 \rightarrow {}^4A_2$ emission is at most only a minor contribution to the broad emission band at 12 700 cm^{-1}.

VIII. CONCLUSIONS

We have prepared a Cr^{3+}-doped glass material (CGGG:Cr^{3+}) with a stoichiometry close to that of the garnet $Ca_3Ga_2Ge_3O_{12}$. It has been found that the material has a high-field Cr^{3+} multisite character. We identified a high-field Cr^{3+} system whose luminescence consists of *R*-line ($^2E \rightarrow {}^4A_2$) emission at 14 480 cm^{-1} accompanied by a broad unstructured sideband that peaks near 12 700 cm^{-1}. High-pressure luminescence spectroscopy up to 150 kbar has shown that the sharp *R* line behaves as expected for a high-field octahedrally coordinated Cr^{3+} center (a redshift of 1.73 cm^{-1}/kbar). The broad emission band, however, did not exhibit the $\sim$10-cm^{-1}/kbar blueshift typically observed for $^4T_2 \rightarrow {}^4A_2$ emission of Cr^{3+}. Instead, it exhibited a redshift of 2 ± 0.5 cm^{-1}/kbar. This shift rate, combined with lifetime decays comparable to those observed for the *R* line, led us to conclude that the broad emission band is not due to the $^4T_2 \rightarrow {}^4A_2$ transition in low-field octahedrally coordinated Cr^{3+} sites. A configurational coordinate diagram developed from luminescence excitation spectra supports this conclusion since it predicts the nearly exclusive existence of high-field sites. Since the broadband and *R*-line emission always appear simultaneously with the same lifetime and pressure coefficients, they must be related to each other. One possibility is to consider the broadband as a phonon-induced sideband of the *R*-line emission. The interaction of odd-parity phonons with Cr^{3+} centers leads to *R*-line sidebands in crystals.[29,30] Usually the sidebands reproduce the structure of lattice phonons. Phonon energies in crystals are typically smaller than 1000 cm^{-1}.[30] Recently, however, Costa *et al.*[31] found that *R*-line sidebands of Cr^{3+} in silicate glasses can extend over a range of 1500 cm^{-1}. In the CGGG:Cr^{3+} glass of this study, the phonon sideband is structureless as expected for a glass, with phonon energies up to about 2000 cm^{-1}.

An additional weak emission band with a peak near 10 300 cm^{-1} was also observed. This emission was attributed to a superposition of the $^4T_2 \rightarrow {}^4A_2$ emission of the low-field Cr^{3+} sites and the emission of chromium ions in

highly valency states (Cr^{4+} and Cr^{5+}). Supporting evidence for the existence of emission from low-field Cr^{3+} sites in the broad 10 300-cm^{-1} emission was obtained in the observation of a weak increase in the *R*-line intensity with increasing pressure upon 488- and 514.5-nm excitations [Figs. 5(b), 5(c), 5(e), 5(f) and Fig. 8]. The weak increase of the *R*-line intensity with pressure is consistent with a pressure-induced electronic crossover from a small fraction of the inhomogeneous low-field Cr^{3+} sites in the CGGG glass used for this study. The contribution of the low-field Cr^{3+} sites to the broad 10 300-cm^{-1} emission band was too small, however, to directly observe its shift behavior with pressure. The observed very small redshift of the 10 300-cm^{-1} emission band with pressure (Fig. 9) indicates that the dominant centers contributing to this emission (Cr^{4+} or Cr^{5+}) are weakly coupled to the glass host. Thus the macroscopic effect of pressure almost does not change the local environment of the center.

The relative contributions of the broad emission bands at 12 700 and 10 300 cm^{-1} to the spectrum were dependent on excitation wavelength. This dependence is readily explained by preferential excitation of lower field sites in the inhomogeneous distribution as the excitation wavelength increases. The excitation wavelength dependent studies also revealed the presence of an additional *R*-line feature at 14 230 cm^{-1}. It is evident from the data that the glass contains a wide range of Cr^{3+} sites with crystal-field strengths ranging from the high field to the low field.

ACKNOWLEDGMENTS

This paper has been supported by II Polish-American Maria Sklodowska–Curie Joint Fund and Gdańsk University (Grant Nos. 5200-5-0299-0, 5200-5-0212-1, and 5200-5-0301-1). Acknowledgment is also made by Y.R.S. and K.L.B. to the Donors of the Petroleum Research Fund, administered by the American Chemistry Society, and to the U.S. National Science Foundation under Grant No. DMR-0107802 for partial support of this research. B.V.P. would like to thank the Polish Jozef Mianowski Found for financial support. The authors would like to thank Dr. Benedykt Kuklinski for performing excitation spectrum measurements.

[1] J. Drube, B. Struve, and G. Huber, Opt. Commun. **50**, 45 (1984).
[2] P. Kenyon, L. Andrews, B. McCollum, and A. Lempicki, IEEE J. Quantum Electron. **18**, 1189 (1982).
[3] D.C. Yeh, W.A. Sibley, M. Suscavage, and M.G. Drexhange, J. Appl. Phys. **62**, 266 (1987).
[4] M. Yamaga, B. Henderson, K.P. O'Donnell, and Y. Gao, Phys. Rev. B **44**, 4853 (1991).
[5] M. Haouari, H. Ben Ouada, H. Maaref, H. Hommel, and A.P. Legrand, J. Phys.: Condens. Matter **9**, 6711 (1997).
[6] M. Haouari, M. Ajroud, H. Ben Ouada, H. Maaref, A. Brenier, and C. Garapon, Phys. Status Solidi B **215**, 1165 (1999).
[7] D.L. Russell, K. Holliday, M. Grinberg, and D.B. Hollis, Phys. Rev. B **59**, 13 712 (1999).
[8] R. Knutson, H. Liu, and W.M. Yen, T.V. Morgan, Phys. Rev. B **40**, 4264 (1989).
[9] C. Ogihara, Y. Gao, K.P. O'Donnell, B. Henderson, and M. Yamaga, J. Phys.: Condens. Matter **4**, 8151 (1992).
[10] D. Jaque, U. Caldino, J.J. Romero, and J. Garcia-Sole, J. Lumin. **83-84**, 477 (1999).
[11] A.E. Nosenko, A.I. Bily, L.V. Kostyk, and V.V. Kravchishin, Opt. Spektrosk. **57**, 837 (1984) in Russian.
[12] M. Grinberg, P.I. Macfarlane, B. Henderson, and K. Holliday, Phys. Rev. B **52**, 3917 (1995).
[13] E. Cavalli, E. Zannoni, and A. Belletti, Opt. Mater. **6**, 153 (1996).
[14] M. Grinberg, P.I. Macfarlane, B. Henderson, and K. Holliday, Phys. Rev. B **52**, 3917 (1995).
[15] M. Grinberg, W. Jaskólski, P.I. Macfarlane, and K. Holliday, J. Phys.: Condens. Matter **9**, 2815 (1997).
[16] P.I. Macfarlane, B. Henderson, K. Holliday, and M. Grinberg, J. Phys.: Condens. Matter **8**, 3933 (1996).
[17] M. Grinberg, J. Barzowska, Y.R. Shen, and K.L. Bray, Phys. Rev. B **63**, 214104 (2001).
[18] J.F. Dolan, L.A. Kappers, and R.H. Bartram, Phys. Rev. B **33**, 7339 (1986).
[19] D. Galanciak, P. Perlin, M. Grinberg, and A. Suchocki, J. Lumin. **60-61**, 223 (1994).
[20] A. Kamińska, A. Suchocki, L. Arizmendi, D. Callejo, F. Jaque, and M. Grinberg, Phys. Rev. B **62**, 10 802 (2000).
[21] A. Kamińska, A. Suchocki, M. Grinberg, J. Garcia-Sole, F. Jaque, and L. Arizmendi, J. Lumin. **87-89**, 571 (2000).
[22] G. Quérel and B. Reynard, Chem. Geol. **128**, 65 (1996).
[23] P.I. Macfarlane, B. Henderson, K. Holliday, and M. Grinberg, J. Phys.: Condens. Matter **8**, 3933 (1996).
[24] M. Grinberg, J. Barzowska, B. Padlyak, T. Nowosielski, B. Kuklinski, and P. Buchynskii, Opt. Appl. **30**, 509 (2000).
[25] B. V. Padlyak and P. P. Buchynskii, Patent of Ukraine, No. UA 25235 A (1998).
[26] B. Padlyak, S. Mudry, V. Halchak, A. Korolyshyn, Yu. Kulyk, and P. Buchynskii, Mol. Phys. Rep. (to be published).
[27] M. Yamaga, B. Henderson, K.P. O'Donnell, and Y. Gao, Phys. Rev. B **44**, 4853 (1991).
[28] B. Henderson and G. F. Imbush, *Optical Spectroscopy of Inorganic Solids* (Clarendon Press, Oxford, 1989).
[29] M. Grinberg, A. Brenier, G. Boulon, C. Pedrini, and C. Madej, J. Lumin. **55**, 303 (1993).
[30] A.P. Vink and A. Meijerink, J. Phys. Chem. Solids **61**, 1717 (2000).
[31] V.C. Costa, F.S. Lammeiras, M.V.B. Pinheiro, D.F. Sousa, L.A.O. Nunes, Y.R. Shen, and K.L. Bray, J. Non-Cryst. Solids **237**, 209 (2000).